Nanoscale Res Lett (2010) 5:61–67
DOI 10.1007/s11671-009-9443-2

NANO EXPRESS

In Situ Generation of Two-Dimensional Au–Pt Core–Shell Nanoparticle Assemblies

Madiha Khalid · Natalie Wasio · Thomas Chase · Krisanu Bandyopadhyay

Received: 8 July 2009 / Accepted: 24 September 2009 / Published online: 14 October 2009

Abstract Two-dimensional assemblies of Au–Pt bimetallic nanoparticles are generated in situ on polyethyleneimmine (PEI) silane functionalized silicon and indium tin oxide (ITO) coated glass surfaces. Atomic force microscopy (AFM), UV–Visible spectroscopy, and electrochemical measurements reveal the formation of core–shell structure with Au as core and Pt as shell. The core–shell structure is further supported by comparing with the corresponding data of Au nanoparticle assemblies. Static contact angle measurements with water show an increase in hydrophilic character due to bimetallic nanoparticle generation on different surfaces. It is further observed that these Au–Pt core–shell bimetallic nanoparticle assemblies are catalytically active towards methanol electro-oxidation, which is the key reaction for direct methanol fuel cells (DMFCs).

Keywords Au–Pt · Bimetallic · Core–shell · Nanoparticle · Cyclic voltammetry · Atomic force microscopy

Introduction

Nanoparticle assemblies have gained significant attention recently with the intention of comprehending the true potential applications of their unique physical, optical, and electronic properties [1]. The ultimate aim is to interface these assemblies to microscale and subsequently to macroscale by organizing them into higher-level structures, devices, and systems with well-defined functionality. Gold–platinum (Au–Pt) bimetallic nanoparticles as alloy [2] or core–shell structure [3], in particular, has attracted increased interest due to its superior performance as fuel cell catalyst over conventional platinum (Pt) based catalyst [4–6]. The major problem for Pt-based catalyst is their poisoning by CO-like intermediates [7, 8]. The unexpected finding of catalytic activity of gold at the nanoscale [9] has opened up various new possibilities of catalyst development and it is well-known today that presence of Au in AuPt system enhances the catalytic activity for electrochemical methanol oxidation reaction (MOR) as a result of electronic interaction between Au and Pt or from the lattice parameter contraction [4]. Currently, these catalysts are mostly synthesized through direct deposition of Pt on the preformed gold nanoparticle (Au NP) seeds in solution [3, 10–13] or on solid supports [14, 15]. However, problem arises from their tendency of coagulation, which occurs due to the unusual high surface energy. While different capping agents such as thiols, amines, phosphines, polymers etc. are normally used in synthesis methods to stabilize and disperse these nanoparticles, interaction with these stabilizing agents may profoundly alter the catalytic properties of these systems [5].

Although assemblies of monometallic nanoparticles are reported extensively [16–19], alloy or core–shell bimetallic nanoparticle has received very limited attention as building blocks until recently. Therefore, new methods of assembling these bimetallic nanoparticles on appropriate surfaces are necessary to integrate them as possible components for future nanodevices or as novel catalysts for fuel cell applications. Early attempt of generating assembly of Au–Pt core–shell nanoparticle (Au–Pt NP) employs the

M. Khalid · N. Wasio · T. Chase · K. Bandyopadhyay (✉)
Department of Natural Sciences, University of Michigan—Dearborn, 4901 Evergreen Road, Dearborn, MI 48128, USA
e-mail: krisanu@umd.umich.edu

deposition of Pt layer onto preformed self-assembled seed Au NPs on silicon surfaces through the reduction of $PtCl_6^{2-}$ in presence of NH_2OH as the mild reducing agent [14]. In another recent approach, Au NP film at the air–water interface was transferred to a solid surface to build a three dimensional nanoporous structure and finally coated with a Pt layer to form the desired core–shell structure [15]. Apart from the limited methods available for assembling core–shell nanoparticles, stabilization against coagulation and fabrication over a large surface area still remains a challenge. As an alternative strategy, nanoparticle assemblies can be generated in situ inside a suitable template on a solid surface to avoid number of sequential steps involved in the methods discussed before. Moreover, the template will essentially act as a reaction chamber that provides scaffold for immobilization of specific metal ions, prevent aggregation, and further act as capping agent to control the growth of the desired nanoparticle structure. It is also possible to create lithographically defined structures of a suitable template to generate nanoparticle patterns without the multiple steps of synthesis and absorption of the corresponding nanoparticles from solution.

In this paper, we report the in situ synthesis of bimetallic core–shell Au–Pt NP assemblies on silicon and indium tin oxide (ITO) coated glass surfaces and also demonstrate that these nanoparticle assemblies are catalytically active towards methanol electro-oxidation which is one of the key electrode reactions in direct methanol fuel cells (DMFCs).

Experimental

Materials

Water used in these experiments was purified though a Millipore system with a resistivity of 18 MΩ cm. Boron doped *p*-type silicon wafers polished on one side (resistivity 10–30 ohm cm) were purchased from Virginia Semiconductor (Fredericksburg, VA). Indium tin oxide (ITO) coated glass substrates were obtained from Delta Technologies, Ltd. (Stillwater, MN) with a resistance of 4–8 Ω. Gold (III) chloride trihydrate ($HAuCl_4{\cdot}3H_2O$), chloroplatinic acid hexahydrate ($H_2PtCl_6{\cdot}6H_2O$), silver nitrate, 200 proof (absolute) ethanol, absolute methanol, and sodium citrate tribasic dihydrate were purchased from Sigma–Aldrich (St. Louis, MO) and were used as received. Trimethoxysilylpropyl modified polyethylenimine (TSPEI) as 50% solution in isopropanol was obtained from Gelest, Inc. (Morrisville, PA) and used without further purification. Concentrated sulfuric acid, 70% nitric acid, and concentrated hydrochloric acids were obtained from Fisher scientific (Pittsburgh, PA).

Surface Functionalization and Nanoparticle Generation

Silicon and ITO surfaces were cleaned before proceeding to surface modification with TSPEI and subsequent nanoparticle formation. Silicon surfaces, cut into required sizes for different characterization, were placed in aqua regia solution (3:1 v/v $HCl:HNO_3$) (*Caution! Aqua regia is a strong oxidizing agent and should be handled with extreme care*) for at least 4 h, rinsed with Millipore water, dried under a stream of argon, and then heated briefly on a hot plate to evaporate any residual water. ITO surfaces were sequentially rinsed in acetone, ethanol, and water, followed by 1.0 M HCl for 10 min and then treated with 1:1:5 (v/v) $H_2O_2:NH_4OH:H_2O$ for an hour. Finally, these surfaces were thoroughly rinsed with Millipore water and dried under flow of argon.

For surface modification, the cleaned samples were immersed in a 2% solution (v/v) of TSPEI in 95% ethanol for 6 min [20]. Surfaces were then rinsed with absolute ethanol, dried under a flow of argon, and left overnight for curing of the silane layer. In a subsequent step, $[AuCl_4]^-$ ion adsorption was done by exposing the surfaces in a 1×10^{-2} M solution of $HAuCl_4{\cdot}3H_2O$ for 8 h followed by rinsing with water and finally drying the surfaces under a flow of argon. In situ reduction to generate Au NPs on the surface was achieved by exposing the above surfaces to a freshly prepared 1% (w/v) aqueous sodium citrate solution for an additional 8 h. For Au–Pt bimetallic core–shell NP generation, 1×10^{-2} M $HAuCl_4$ and 1×10^{-2} M H_2PtCl_6 solutions were made separately and mixed in different volumes to create the desired Au:Pt mole ratio in the final solution, ranging from 1:0,1:0.25, 1:0.75 to 1:1. After incubating the surface for 8 h, rinsing with water and drying under flow of argon, surfaces with adsorbed ions were placed in a freshly prepared 1% (w/v) aqueous solution of sodium citrate for 8 h to generate the Au–Pt NPs.

Characterization of the Nanoparticle Assemblies

Contact angle was measured by Pocket Goniometer, PG-1 model (Paul N. Gardner Company Inc., Pompano Beach, FL), which is a battery-operated instrument for manual measurements of static contact angles at "equilibrium." The plunger was filled with Millipore water, which was slowly pressed out until it formed a droplet on the surface (1.5 cm wide × 2.5–3.0 cm long). At least five different spots were chosen for measuring the contact angle for each surface and an average of the values was reported.

UV–visible spectra of gold nanoparticles on ITO surfaces were collected using USB4000-UV-VIS spectrophotometer from Ocean Optics (Dunedin, FL). Surfaces with nanoparticles were directly introduced into the cuvette

holder (1 cm path length) and spectra were recorded with corresponding clean unmodified surface as the reference.

Atomic force microscopy (AFM) imaging was performed using Veeco (Santa Barbara, CA) Multimode system, equipped with a Nanoscope IIIa controller, in tapping mode. Cantilevers were phosphorous-doped silicon specific for tapping mode imaging. The local root-mean-square (RMS) surface roughness was determined using height data from at least four representative 2 μm × 2 μm scan areas through roughness analysis program included in the AFM analysis software. Surface coverage of different nanoparticles was estimated by analyzing the mean grain area and number of grains present in a typical 2 μm × 2 μm (total area = 4 μm^2) AFM image of the respective nanoparticle.

Cyclic voltammetric (CV) measurements were performed in a Teflon® electrochemical cell (3 ml maximum volume) using standard three-electrode configuration, which was controlled by a CHI660C electrochemical workstation (CH Instruments, Inc. Austin, TX). A coiled platinum wire was used as the counter electrode, aqueous Ag/AgCl was used as the reference electrode, and ITO surfaces were used as the working electrodes.

Results and Discussion

Scheme 1 shows the different steps involved in the generation of bimetallic core–shell Au–Pt NPs by simultaneous in situ reduction of $[AuCl_4]^-$ and $[PtCl_6]^{2-}$ ions bound to the TSPEI functionalized surface. The multiple amine functionalities present at the polyethyleneimine (PEI) backbone of TSPEI can entrap both $[AuCl_4]^-$ and $[PtCl_6]^{2-}$ ions from solution through electrostatic interaction at a lower pH. The surface functionalization with TSPEI is achieved through the well-known silane coupling chemistry of the trimethoxysilane groups present at one end of the molecule. Two different kinds of surfaces are used in our experiments with an idea that atomically smooth silicon is ideal for structural characterization of the surface bound nanoparticles by AFM, while the conducting ITO surfaces are suitable to assess the optical and electrocatalytic activity of the formed nanostructures. Figure 1a shows a representative AFM image of nearly uniform spherical Au–Pt NPs on silicon surface after the final reduction step with the Au:Pt mole ratio of 1:1 in the final solution. A larger scan size of 5 μm × 5 μm in Fig. 1b illustrates the formation of Au–Pt NP assembly over a larger area, without much long range ordering. An average height of 7.4 ± 1.3 nm is obtained for the Au–Pt NPs from the analysis of a number of AFM images of different samples which is evident from the histogram in the inset of Fig. 1a. Comparison of monometallic Au NPs generated by the same procedure shows an average height of 6.3 ± 1.2 nm with a more densely packed structure (Fig. 1c, inset). It is known that colloidal metal nanoparticles in solution are generated through consecutive steps of nucleation and growth. The balance between the rate of nucleation and growth can affect the final particle size. It is observed that fast nucleation step leads to smaller particles and slow nucleation results in larger particles. The growth step can occur mainly by consuming molecular precursors from the surrounding solution or by Ostwald ripening when large particles grow at the expense of dissolving a smaller one. For colloidal metal nanoparticle growth in solution, Ostwald ripening is mostly absent and the growth usually happens due to consumption of dissolved metal precursors from solution. In addition, the fast nucleation event and following growth step must be completely separate in order to achieve narrow size distribution of the final nanoparticles while multiple nucleation events may lead to wide size distribution [21, 22]. The current situation of in situ nanoparticle generation is different from solution synthesis since the molecular precursor ($[AuCl_4]^-$) is attached to the template on the surface and no free precursor is essentially present during nucleation and growth step (during citrate reduction). The observed Gaussian distribution of particle size for both Au and Au–Pt systems indicates a single and fast nucleation event followed by the growth step through consumption of the surface bound molecular precursor. The increase in size during bimetallic NP formation compared to its monometallic constituent has been reported in the literature in the context of core–shell structure formation in solution [3, 11] and the increase is expected from the relation [13]

$$D_{\text{core@shell}} = D_{\text{core}}\left(1 + \frac{V_{\text{shell}}C_{\text{shell}}}{V_{\text{core}}C_{\text{core}}}\right)^{1/3} \quad (1)$$

where V is the corresponding mole volumes, C is the overall concentration of the specific metal involved, and D is the diameter. Alternatively, rather densely packed assembly generated for Au NPs compared to Au–Pt NPs is possibly due to the reduction in the number of surface adsorbed ions during bimetallic NP formation, considering the difference in ionic charges of the respective ions and electrostatic interactions working in the process.

Water contact angle measurements are used to follow the change in surface character during different steps of Au–Pt NP generation on the surface. Figure 1d shows the overall trend in the contact angle change from bare silicon surface to the nanoparticle formation on the surface for Au:Pt mole ratio of 1:1 in the final solution. Contact angle increased from 25 ± 2.1° for bare silicon to 54 ± 0.5° with adsorbed $[AuCl_4]^-$ and $[PtCl_6]^{2-}$ on the surface and eventually decreased to 34 ± 0.57° due to formation of Au–Pt NPs after the reduction step. This indeed implies the

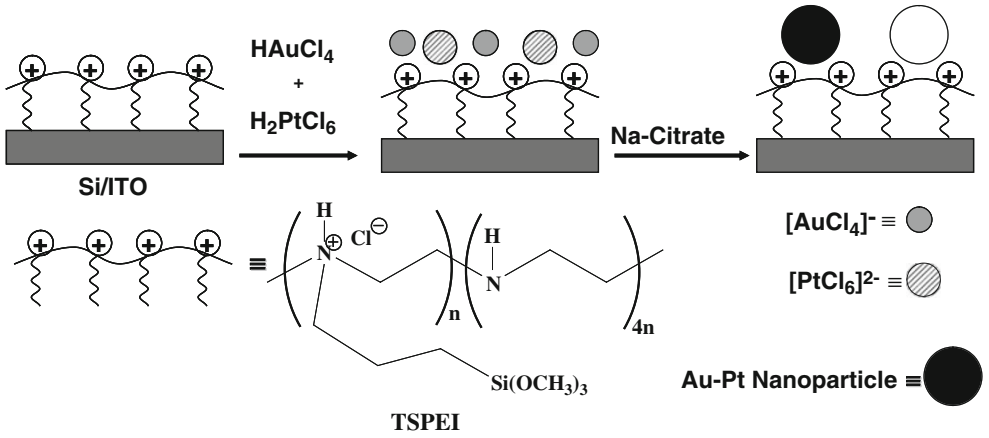

Scheme 1 Steps involved in generating Au–Pt bimetallic core–shell nanoparticles on silicon or ITO surfaces. Structure of trimethoxysilylpropyl modified polyethylenimine (TSPEI) is also shown

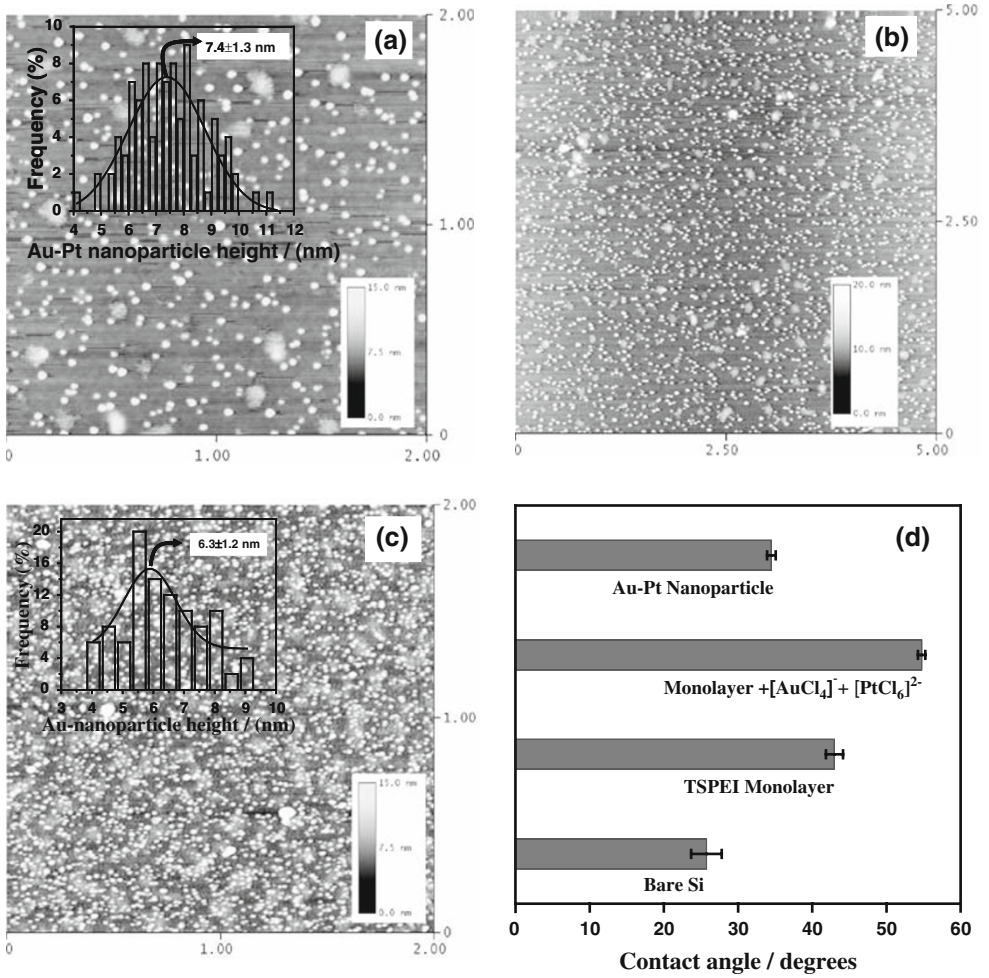

Fig. 1 **a** 2μm × 2μm and **b** 5μm × 5μm tapping mode AFM height image of in situ generated bimetallic Au–Pt NPs (Au:Pt mole ratio = 1:1) on TSPEI modified surface. **c** 2μm × 2μm AFM height image of monometallic Au NPs generated on TSPEI modified surface. Inset of (**a**) and (**c**) show the respective histogram of the Au–Pt and Au nanoparticle height distribution with a fit (*solid line*) using Gaussian distribution function after analyzing a number of AFM images. Respective mean height and standard deviation are also shown. **d** Change in static water contact angle at different steps of Au–Pt NP formation

enhanced hydrophilic character of the surface due to nanoparticle formation. A similar trend in change of hydrophilic/hydrophobic character has been observed for Au NP formation on the surface by the present method and also reported in the literature for Ag NP formation [23, 24]. Controlling the hydrophilic and hydrophobic properties of a surface is significant due to different potential application areas like self-cleaning surfaces and sensors.

The earlier discussion of AFM results points to the possible core–shell structure formation during in situ synthesis of Au–Pt NPs on the surface from the observed increase in nanoparticle size going from pure Au NPs to Au–Pt NPs. However, it is not obvious which metal constitute the core and which one the shell and further experimental evidence is required to elucidate the actual structure of these bimetallic Au–Pt NPs generated on the surface. UV–Visible spectroscopy has proven to be a versatile technique to understand the structure of core–shell Au–Pt NPs generated in solution and the results are well documented in the literature [3, 10, 25]. Hence, we synthesized Au NPs and Au–Pt NPs on transparent ITO surfaces to assess their optical property, using the same methodology as discussed above. Figure 2 shows the comparison of the UV–Visible response of pure Au NPs to that of Au–Pt NPs with different mole ratio of Au and Pt. It is evident that Au NPs show a characteristic plasmon absorption band at 558 nm. Interestingly, the Au surface plasmon peak for Au–Pt NPs shifted to lower wavelength (at 548 nm) for a mole ratio of Au:Pt = 1:0.25 and further blue shifted (a broad peak centered at 538 nm) with increased Pt content at a ratio of Au:Pt = 1: 0.75. Finally, the surface plasmon peak for Au completely disappears for Au:Pt = 1:1. These results, along with several earlier reports of Au–Pt NP formation in solution [3, 5, 10, 25–27] substantiate that the deposition of a Pt shell on top of an Au core is responsible for the disappearance of the Au surface plasmon peak in the UV–Visible absorption spectrum. In order to confirm the presence of the Pt shell, Au–Pt nanoparticles (Au:Pt = 1:1) are generated on quartz surface (transparent to UV) which shows a surface plasmon peak ~222 nm (Fig. 2b) corresponding to zero-valent platinum [28]. The present results indeed demonstrate the formation of Au–Pt core–shell NPs on the solid surface and are particularly significant since the core and the shell are generated in situ unlike the previous reports in solution where core particles were initially synthesized and the shell was deposited subsequently.

In order to further confirm the core–shell structure of these Au–Pt NPs, electrochemical measurements are done with Au–Pt NP assemblies generated on ITO surfaces in aqueous KOH solution and compared to Au NP assemblies generated on ITO surfaces. Detection of gold oxide (AuO_x) from oxidation/reduction waves in basic (0.5 M KOH)

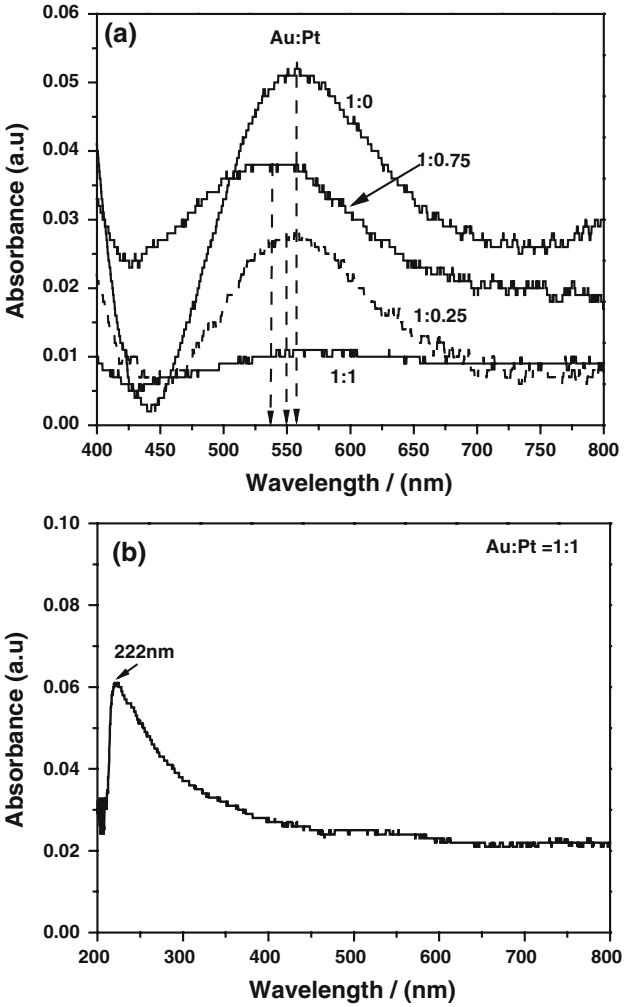

Fig. 2 **a** UV–Visible spectrum for Au–Pt bimetallic NPs generated on ITO surface with varying mole ratio of Au:Pt. Corresponding Au:Pt ratios are shown on the individual spectrum. **b** UV–Visible spectrum for Au–Pt bimetallic NPs generated on quartz surface with 1:1 mole ratio of Au:Pt

medium during cyclic voltammetry measurements can provide information about the chemical nature of the shell. Figure 3a shows superimposed cyclic voltammograms for Au NPs and Au–Pt NPs generated on ITO surface in 0.5 M KOH solution. The presence of oxidation/reduction waves of AuO_x at ~0.24 V for Au NPs, in contrast to the absence of such peak for Au–Pt NPs suggests that the oxidation/reduction of Au is suppressed by the Pt shell [3] in the latter, which again validate the core–shell structure of the present in situ generated Au–Pt NPs. To explore the catalytic properties of these Au–Pt NP bound ITO surfaces towards methanol oxidation reaction (MOR), cyclic voltammetric responses (Fig. 3b) are recorded in 0.5 M KOH in presence and absence of MeOH. A strong anodic peak at ~+0.65 V (relative to aqueous Ag/AgCl reference electrode) is observed, corresponding to methanol electro oxidation [29]. However, this anodic peak disappears in

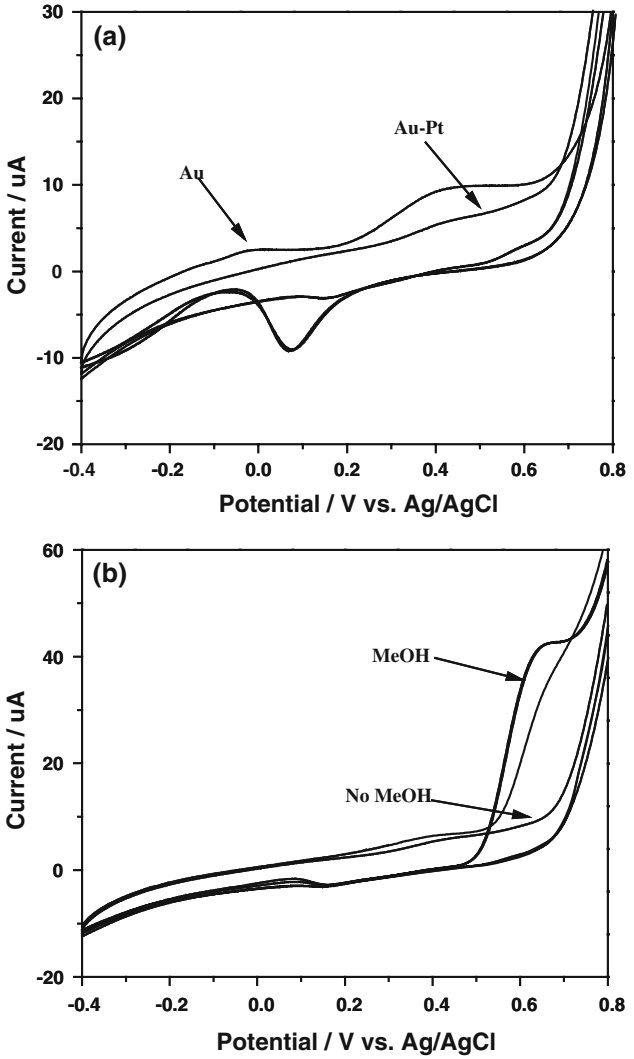

Fig. 3 **a** Cyclic voltammetric response of Au NP and Au–Pt NP assemblies on ITO surface in 0.5 M KOH. **b** Electro-catalytic oxidation of methanol at the Au–Pt NP assembly on ITO surface in 0.5 M KOH with and without 5.0 M methanol. Scan rate = 50 mV/s and electrode area = 0.5 cm^2

absence of methanol in solution. It is to be noted that these Au–Pt NP-bound ITO surfaces were not thermally activated before assessing their catalytic property.

Generation of Au–Pt core–shell structure from simultaneous reduction of surface bound $[AuCl_4]^-$ and $[PtCl_6]^{2-}$ ions, evident from the UV–Visible and electrochemical results presented above and the preferred elemental distribution of the core and shell materials warrant further discussion. Since the formation of nanoparticles in solution essentially proceeds through nucleation and growth steps, it is expected that the metal ion which is easier to reduce will nucleate first and serve as the nucleation site for the second one during simultaneous reduction of the two metal ions in solution. In this case, platinum will have to be first reduced to Pt^{2+} from Pt^{4+} and then to Pt^0 with a standard redox potential of 0.775 V for $[PtCl_6]^{2-}/[PtCl_4]^{2-}$ and 0.68 V for $[PtCl_4]^{2-}/Pt^0$ compared to a single step reduction for gold from Au^{3+} to Au^0 with a standard reduction potential of 1.002 V for $[AuCl_4]^-/Au^0$, reported at room temperature [25]. Considering the reduction potentials, it is obvious that Au will preferably nucleate first to form the core followed by Pt to form the shell. However, the situation for surface bound ions is rather different as the respective ions are pinned down to the surface through electrostatic attraction of the template and will have limited mobility. The underlying mechanism of in situ core–shell structure formation on the surface is a subject of our on-going investigation.

Conclusions

In summary, we have reported an elegant method for in situ generation of two-dimensional Au–Pt bimetallic nanoparticle assemblies on solid surfaces functionalized with polyethyleneimine template. AFM results reveal the formation of Au–Pt NP assemblies on silicon surface without much long range ordering and also show an increase in size of these bimetallic nanoparticles compared to their monometallic Au equivalents. Comparison of UV–Visible and electrochemical response of Au–Pt NPs to that of Au NPs generated on ITO surfaces authenticate the core–shell structure of these bimetallic nanoparticles. Moreover, these Au–Pt NP assemblies are active towards methanol oxidation, demonstrating their potential as catalyst for DMFCs. This in situ synthetic approach relies on self-assembly employing wet chemical technique at an ambient condition and can also be extended to create other bimetallic NP assemblies. Further, it offers a flexible method to generate bimetallic core–shell NPs for site selective deposition, nanoparticle patterning for nanoelectronic applications and can also be combined with the conventional lithographic techniques.

Acknowledgments We thank the American Chemical Society, Petroleum Research Fund (ACS-PRF) and National Science Foundation (NSF) for financial support. Office of the Vice President for Research (OVPR), UM-Ann Arbor and the Office of Research and Sponsored Programs, UM-Dearborn are also gratefully acknowledged for additional funding.

References

1. S.G. Orlin, D. Velev, Adv. Mater. **21**, 1897 (2009)
2. J. Luo, P.N. Njoki, Y. Lin, D. Mott, L. Wang, C.-J. Zhong, Langmuir **22**, 92 (2006)
3. J. Luo, L. Wang, D. Mott, P.N. Njoki, Y. Lin, T. He, Z. Xu, B.N. Wanjana, I.-I.S. Lim, C.-J. Zhong, Adv. Mater. **20**, 4342 (2008)
4. J. Zeng, J. Yang, J.Y. Lee, W. Zhou, J. Phys. Chem. B **110**, 24606 (2006)

5. H.-P. Liang, T.G.J. Jones, N.S. Lawrence, L. Jiang, J.S. Barnard, J. Phys. Chem. C **112**, 4327 (2008)
6. J.B. Park, S.F. Conner, D.A. Chen, J. Phys. Chem. C **112**, 5490 (2008)
7. U.A. Paulus, U. Endruschat, G.J. Feldmeyer, T.J. Schmidt, H. Bönnemann, R.J. Behm, J. Catal. **195**, 383 (2000)
8. E. Antolini, Mater. Chem. Phys. **78**, 563 (2003)
9. M. Haruta, Catal. Today **36**, 153 (1997)
10. A. Henglein, J. Phys. Chem. B **104**, 2201 (2000)
11. I.-S. Park, K.-S. Lee, D.-S. Jung, H.-Y. Park, Y.-E. Sung, Electrochim. Acta **52**, 5599 (2007)
12. L. Wang, B. Qi, L. Sun, Y. Sun, C. Guo, Z. Li, Mater. Lett. **62**, 1279 (2008)
13. L. Lu, G. Sun, H. Zhang, H. Wang, S. Xi, J. Hu, Z. Tian, R. Chen, J. Mater. Chem. **14**, 1005 (2004)
14. L. Cao, L. Tong, P. Diao, T. Zhu, Z. Liu, Chem. Mater. **16**, 3239 (2004)
15. Y.-K. Park, S.-H. Yoo, S. Park, Langmuir **24**, 4370 (2008)
16. H. Xu, R. Hong, X. Wang, R. Arvizo, C. You, B. Samanta, D. Patra, M.T. Tuominen, V.M. Rotello, Adv. Mater. **19**, 1383 (2007)
17. O.P. Khatri, K. Murase, H. Sugimura, Langmuir **24**, 3787 (2008)
18. L.B. Haoguo Zhu, S.M. Mahurin, G.A. Baker, E.W.H. Sheng Dai, J. Mater. Chem. **18**, 1079 (2008)
19. L.E. Russell, A.A. Galyean, S.M. Notte, M.C. Leopold, Langmuir **23**, 7466 (2007)
20. M. Khalid, I. Pala, N. Wasio, K. Bandyopadhyay, Colloids Surf. A: Physicochem. Eng. Aspects. **348**, 263 (2009)
21. A. Kirsten, H. Hauke, K. Andreas, A.C.B. Jose, W. Horst, Adv. Funct. Mater. **18**, 3850 (2008)
22. E.V. Shevchenko, D.V. Talapin, H. Schnablegger, A. Kornowski, O. Festin, P. Svedlindh, M. Haase, H. Weller, J. Am. Chem. Soc. **125**, 9090 (2003)
23. M. Riskin, B. Basnar, V.I. Chegel, E. Katz, I. Willner, F. Shi, X. Zhang, J. Am. Chem. Soc. **128**, 1253 (2006)
24. M. Riskin, E. Katz, V. Gutkin, I. Willner, Langmuir **22**, 10483 (2006)
25. D.I. Garcia-Gutierrez, C.E. Gutierrez-Wing, L. Giovanetti, J.M. Ramallo-Lopez, F.G. Requejo, M. Jose-Yacaman, J. Phys. Chem. B **109**, 3813 (2005)
26. M.-L. Wu, D.-H. Chen, T.-C. Huang, Chem. Mater. **13**, 599 (2001)
27. W. Zhang, L. Li, Y. Du, X. Wang, P. Yang, Catal. Lett. **127**, 429 (2009)
28. M.H. Ullah, C. Won-Sub, K. Il, H. Chang-Sik, Small **2**, 870 (2006)
29. J. Luo, M.M. Maye, N.N. Kariuki, L. Wang, P. Njoki, Y. Lin, M. Schadt, H.R. Naslund, C.-J. Zhong, Catal. Today **99**, 291 (2005)